Microwave Engineering
Ulm University

universität ulm

# Instantaneous Ego-Motion Estimation based on Ambiguous Velocity Information within a Network of Radar Sensors

Timo Grebner, Pirmin Schoeder, Fabian Konrad, and Christian Waldschmidt


DOI: 10.1109/LMWC.2022.3145661

# Instantaneous Ego-Motion Estimation based on Ambiguous Velocity Information within a Network of Radar Sensors

Timo Grebner[#1], Pirmin Schoeder[#], Fabian Konrad[#], Christian Waldschmidt[#]
[#]Institute of Microwave Engineering, Ulm University, Germany
[1]timo.grebner@uni-ulm.de

***Abstract*— Accurate ego-motion estimation plays a crucial role in the automotive sector, as well as in the field of robotics for both the representation of the environment, as grid-maps e.g., as well as the estimation of target features. Radar-based ego-motion estimations show great potential but are limited by their maximum detectable unambiguous radial velocity. This limitation becomes even worse with the often used TDM-MIMO multiplexing strategy. The following paper presents a radar-based ego-motion estimation algorithm, which overcomes this limitation. The presented approach is independent of modulation scheme or front-end design and expands the maximum estimable vehicle speed.**

***Keywords*— ego-motion, radar systems, frequency modulated continuous wave (FMCW), speed disambiguation**

## I. Introduction

In recent decades, environmental perception, both for robotics and automotive, has become increasingly important with respect to self-localization. Especially for short-time prediction, high-precision ego-motion information can be used for this purpose [1], [2]. A wide variety of sensor principles can be used for ego-motion estimation, each with their individual advantages in specific scenarios. One commonly used system is the differential global positioning systems (D-GPS). However, high-accuracy D-GPS has severe accuracy limitations in densely built-up areas and relies on external infrastructure. Sensor systems not relying on external infrastructure that overcome this disadvantage are wheel speed sensors, LIDAR systems, or radar systems [3]. While wheel speed sensors provide very precise speed estimates, they provide incorrect speed information in case of slippage. LIDAR on the other hand is susceptible to environmental optical effects. In contrary, radar sensors can reliably and instantaneously determine the vehicle's own speed almost independently of external conditions. In [4], it was shown that radar sensors can be used to reliably determine ego-motion based on stationary targets. The performance of ego-motion estimation can further be improved by the use of radar networks [5], [6].

However, due to physical limitations, chirp-sequence radar sensors are limited with respect to their maximum unambiguously measurable velocity [7]. This leads to the fact that the maximum detectable ego-motion velocity is also limited. Different approaches to resolve the ambiguities of velocities for TDM-MIMO chirp-sequence radar sensors have been shown in [7] and [8]. However, these algorithms are limited by the antenna positions [9] or the disambiguation [7].

The algorithm presented in this paper enables instantaneous ego-motion estimation at velocities multiple times higher than the unambiguous detectable radial velocity of the radar system and is applicable for both SIMO and MIMO radar sensors, independent of modulation and antenna design.

For this purpose, in Section II, the basics of ego-motion estimation are derived. The problems of existing approaches are discussed, and multiple approaches to overcome those problems for SIMO as well as MIMO radar sensors are presented. The subsequent measurements in Section III illustrate the functionality and robustness of the presented algorithm based on measurements in road traffic.

## II. Sensor-Setup and Ego-Motion Estimation

Radar sensors provide a highly accurate radial velocity measurement, which can be measured between $N$ radar sensors and each of the $M_n$ detected targets ($n \in N$). Based on the radial velocity of static targets, a precise motion estimate of the radar sensor, and therefore the vehicle, can be determined. In general, the motion of a vehicle can be described by the two velocity components $v_x$, $v_y$ and the yaw rate $\omega$. This is shown in Fig. 1.

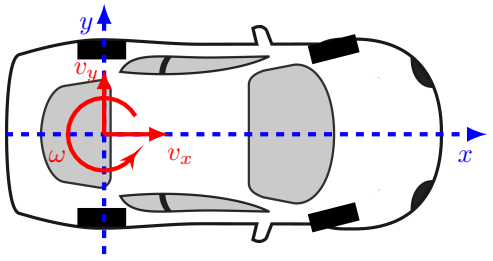


Fig. 1. Vehicle coordinate system in blue, dashed and velocity coordinate system in red, solid lines.

These three velocity components can be determined using at least two radar sensors [5], and the corresponding target lists are comprising the information angle of arrival (AoA) and radial velocity. A signal flow chart is shown in Fig. 2.

The blue boxes in Fig. 2 illustrate the basic structure of the ego-motion estimation algorithm according to [5]. The raw data from $N$ externally triggered chirp-sequence radar sensors

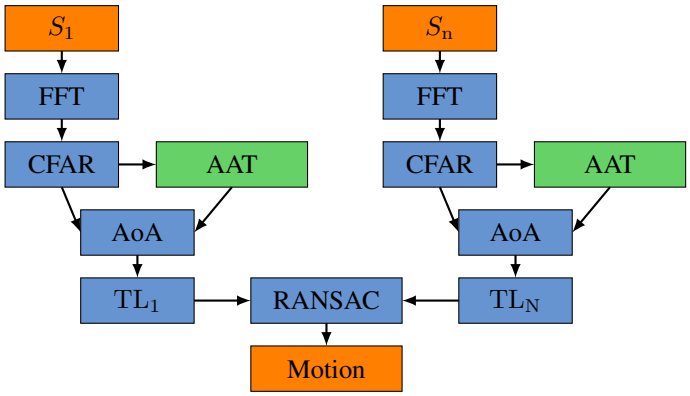


Fig. 2. Signal flow graph of a general radar network-based ($S_1, ..., .S_n$) ego-motion estimation (blue), enhanced by artificially added target (AAT) ambiguities (green) and subsequent ambiguity elimination.

is stored, processed independently, and transformed into the frequency domain using a 2D fast Fourier transform (FFT). The relevant target information is extracted by using a constant false alarm rate (CFAR), subsequent peak detection, and angle of arrival (AoA) estimation. Based on these target lists, the following model can be constructed [4]:

$$\underbrace{\begin{bmatrix} -v^{\mathrm{r}}_{n,1} \\ -v^{\mathrm{r}}_{n,2} \\ \vdots \\ -v^{\mathrm{r}}_{n,M} \end{bmatrix}}_{\mathbf{V}^{\mathrm{r}}_n} = \underbrace{\begin{bmatrix} \cos(\phi_{n,1}) & \sin(\phi_{n,1}) \\ \cos(\phi_{n,2}) & \sin(\phi_{n,2}) \\ \vdots & \\ \cos(\phi_{n,M}) & \sin(\phi_{n,M}) \end{bmatrix}}_{\mathbf{D}_n} \cdot \underbrace{\begin{bmatrix} -y^{\mathrm{s}}_n & 1 & 0 \\ x^{\mathrm{s}}_n & 0 & 1 \end{bmatrix}}_{\mathbf{S}_n} \cdot \begin{bmatrix} \omega \\ v_x \\ v_y \end{bmatrix}. \tag{1}$$

Here, $\phi_{n,m}$ describes the sum of local AoA and sensor orientation, $v^{\mathrm{r}}_{n,m}$ the radial velocity, as well as $x^{\mathrm{s}}_n$ and $y^{\mathrm{s}}_n$ the position of the sensors of the $m$-th target and the $n$-th sensor. Thereby, the matrix $\mathbf{V}^{\mathrm{r}}_n$ consists of all measured radial velocities between the non-stationary sensor $n$ and the stationary and non-stationary targets in the channel. As soon as a sensor network is used, the equation can be converted to

$$\underbrace{\begin{bmatrix} \mathbf{V^r_1} \\ \mathbf{V^r_2} \\ \vdots \\ \mathbf{V}^r_N \end{bmatrix}}_{\mathbf{V^r}} = \underbrace{\begin{bmatrix} \mathbf{D_1} \cdot \mathbf{S_1} \\ \mathbf{D_2} \cdot \mathbf{S_2} \\ \vdots \\ \mathbf{D}_N \cdot \mathbf{S}_N \end{bmatrix}}_{\mathbf{M}} \cdot \underbrace{\begin{bmatrix} \omega \\ v_x \\ v_y \end{bmatrix}}_{\mathbf{V_P}}. \tag{2}$$

Equation (2) can be solved for the desired ego-motion vector $\mathbf{V_P}$ in the least square-sense by the aids of the Moore-Penrose inverse of matrix $\mathbf{M}$. In [4], [5], and [6] it was shown that the ego-motion can be estimated with high accuracy. The selection of stationary targets is done using a random sample consensus (RANSAC) algorithm.

### A. Velocity Error

As soon as the occurring radial velocities $v^{\mathrm{r}}_{n,m}$ are higher than the maximum unambiguously detectable radial velocities

$$|v^{\mathrm{r}}_{\mathrm{max}}| = \frac{c_0}{4 f_{\mathrm{c}} T_{\mathrm{r}}}. \tag{3}$$

the estimation is no longer successful [10]. $T_{\mathrm{r}}$ indicates the ramp period and $f_{\mathrm{c}}$ the start frequency of the ramp. The measured radial velocity $v^{\mathrm{r}}_{\mathrm{d}}$ deviates from the real radial velocity $v^{\mathrm{r}}_{\mathrm{th}}$ for targets exceeding (3). The relation between $v^{\mathrm{r}}_{\mathrm{d}}$ and $v^{\mathrm{r}}_{\mathrm{th}}$ is described by

$$v^{\mathrm{r}}_{\mathrm{d}} = \mathrm{mod}\left(v^{\mathrm{r}}_{\mathrm{th}} + v^{\mathrm{r}}_{\mathrm{max}}, 2v^{\mathrm{r}}_{\mathrm{max}}\right) - v^{\mathrm{r}}_{\mathrm{max}} \tag{4}$$

From (4), it is obvious that independent of the actual velocity, all detected velocities are mapped to the interval $[-v^{\mathrm{r}}_{\mathrm{max}}, v^{\mathrm{r}}_{\mathrm{max}}]$.

### B. Angle of Arrival Error

Depending on the antenna configuration and multiplexing strategy, an incorrect radial velocity estimate can lead to incorrect angle estimates. While for SIMO radar sensors only the radial velocities are estimated incorrectly, for TDM-MIMO radar sensors both the radial velocities and the corresponding angles are estimated wrongly [7]. The sequential activation of the individual transmitters results in the signals of the individual sub-apertures being acquired at different times, leading to phase errors depending on the target speed. These phase errors can be compensated if the real radial velocity is known [8]. The number of transmit antennas correlates with the number of phase correction terms.

### C. Ambiguity Resolving

Since no statement can be made about each target $m_n$ whether it has correct target properties (AoA and radial velocity) or ambiguities, all possible target ambiguities are first calculated and included in the target list. However, since not every added ambiguity represents a real target, incorrect targets must then be distinguished from real targets. In the first step, all targets including all target properties are duplicated $2K$ times. Hereby, each target exists $2K + 1$ times in the target lists $\mathrm{TL}_n$, which is exemplary shown for the target $n$ of the sensor $m$:

$$\begin{bmatrix} v^{\mathrm{r}}_{\mathrm{d}} \\ \phi_{\mathrm{d}} \end{bmatrix} \rightarrow \begin{bmatrix} v^{\mathrm{r}}_{\mathrm{a-K}} & v^{\mathrm{r}}_{\mathrm{a-K+1}} & \cdots & v^{\mathrm{r}}_{\mathrm{aK-1}} & v^{\mathrm{r}}_{\mathrm{aK}} \\ \phi_{\mathrm{a-K}} & \phi_{\mathrm{a-K+1}} & \cdots & \phi_{\mathrm{aK-1}} & \phi_{\mathrm{aK}} \end{bmatrix} \tag{5}$$

Here, $K$ denotes the number of added ambiguities, $v^{\mathrm{r}}_{\mathrm{d}}$ and $\phi_{\mathrm{d}}$ the detected target properties, and $v^{\mathrm{r}}_{\mathrm{a_k}}$ and $\phi_{\mathrm{a_k}}$ the artificially added $k$-th ambiguity $k \in [-K, K]$. The variable $K$ should be chosen at least such that the highest radial velocity is approximately equal to the maximum vehicle velocity and $v^{\mathrm{r}}_{\mathrm{aKm}} \approx \max(v_x)$ holds. There is no maximum value for $K$, but the computational complexity of the RANSAC algorithm applied here scales with the factor $K$. The ambiguous velocities can be calculated with the help of (4) according to

$$v^{\mathrm{r}}_{\mathrm{a_k}} = v^{\mathrm{r}}_{\mathrm{d}} + 2|v^{\mathrm{r}}_{\mathrm{max}}|k \tag{6}$$

which is shown in green in Fig. 2. Based on the determined ambiguous radial velocities, the method described in [7] can be used to determine the corresponding ambiguous angles $\phi_{\mathrm{a_k}}$. In the case of SIMO radar sensors, this step can be neglected since AoA of SIMO radar sensors can be uniquely determined

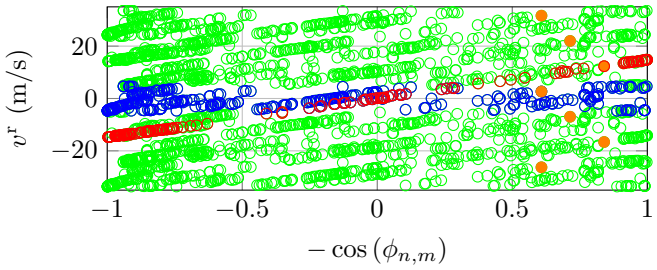


Fig. 3. Illustration of the speed disambiguation algorithm with detected targets $v_{\mathrm{d},n,m}$. Exemplary illustration of $2K$ ambiguously added targets based on one exemplary $v_{\mathrm{d},n,m}$ and for all detected targets $v_{\mathrm{a},n,m}$. RANSAC-based filtered stationary ambiguous-free targets used for ego-motion are displayed in red.

independently of the velocity ambiguities. An illustration of this principle is shown in Fig. 3 for a straight-line drive frame from Section IV.

The blue circles denote the detected targets' $v_{\mathrm{d},n,m}$, which are all in the interval $\pm v^{\mathrm{r}}_{\max}$. For an example point $(0.608|2.676)$, $K$=3 ambiguities are added, which is represented by the orange circles, based on which both the ambiguous velocities and the ambiguity in angle are visible. The green scatter points in Fig. 3 symbolize all $v_{\mathrm{a},n,m}$ generated ambiguities according to (5).

From the $v_{\mathrm{a},n,m}$ existing targets, those targets have to be filtered out, whose ambiguities can be correctly resolved and which can be used for the velocity estimation. Similar to the velocity estimation with unambiguous radial velocity measurements, a RANSAC algorithm is used for this purpose. However, this algorithm must filter out not only non-stationary targets and false detections but also all artificially added ambiguities.

Since even in the optimal scenario (no false detections and no non-stationary targets), only every $2K$+1-th target of the vehicle motion is suitable, enough RANSAC iterations should be performed to ensure a robust and error-free ego-motion estimation. The stationary targets that were filtered out using the RANSAC algorithm are shown as red circles in Fig. 3. Based on these stationary and ambiguity-free targets, ego-motion can then be estimated a priori-free using (2).

## III. Measurement Setup

The measurement setup to validate the presented methods is shown in Fig. 4 and consists of an incoherent radar network with four chirp-sequence radar sensors.

Fig. 4. Experimental system setup with four radar sensors on a car.

Table 1. Used Radar Parameters for Ego-Motion Estimation.

| **Parameter** | **Value** | | | |
|---|---|---|---|---|
| | $S_1$ | $S_2$ | $S_3$ | $S_4$ |
| Start frequency $f_{\mathrm{start}}$ (GHz) | 77.22 | 77.25 | 77.28 | 77.34 |
| Bandwidth $B$ | 1.02 GHz | | | |
| Ramp repetition time $T_{\mathrm{r}}$ | 67 µs | | | |
| Sampling frequency $f_{\mathrm{s}}$ (IQ) | 10 MHz | | | |
| Number of ramps (per Tx) | 128 | | | |
| Max. unambiguous velocity | 4.823 m/s | | | |
| Number of transmitters | 3 | | | |
| Number of receivers | 4 | | | |
| Measurement rate | 30 Hz | | | |

In order to measure realistic scenarios and participate in road traffic, the sensors were mounted on the car roof for regulatory reasons. An external trigger is used for the time synchronization of the sensors. In combination with a shift of the start frequency, interference between the sensors is suppressed. The sensors have an orientation of approximately 0°, 90°, 180°, and 270° to provide a 360° field of view (FoV). The radar parameters are listed in Table 1.

The ground truth velocity was determined by means of a tachymeter [11]. Since only a one-dimensional velocity estimate in the $x$-direction can be determined with this tachymeter, $v_y$=0 m/s is assumed for the velocity, since the vehicle had negligible movement in $y$-direction.

## IV. Measurement Results

The results of two measurements are shown in the following figures. The result of the speed estimation of a fast straight drive is shown in Fig. 5.

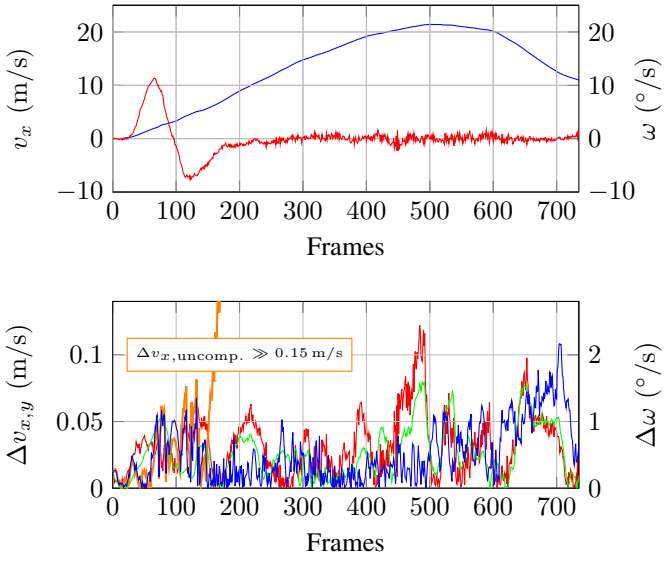


Fig. 5. Straight line drive at high speed. Ground truth velocity (top), estimation error (bottom) with $v_x$, $v_y$, and $\omega$. $v_{x,\mathrm{uncomp}}$ without velocity correction described in this paper, thus according to [5].

Fig. 5a shows the ground truth $v_x$ velocity and yaw rate $\omega$. The error of the radar-based 3 dimensions of freedom (DoF) ego-motion estimation for the searched velocity components, $v_x$, $v_y$, and $\omega$ are shown in Fig. 5b. Although the maximum

radial velocity that can be uniquely determined in this radar mode is $4.82\,\mathrm{m/s}$ for each radar sensor, vehicle velocities, in both the $x$- and $y$-directions of greater than $21\,\mathrm{m/s}$ can be reliably determined with an RMSE less than $0.03\,\mathrm{m/s}$. Similarly, the RMSE of the yaw rate is only $0.9\,^\circ/\mathrm{s}$.

Fig. 5b also shows the error $\Delta v_{x,\mathrm{uncomp.}}$ (without velocity correction described in this paper), which is identical up to frame 150. However, the speed estimation according to [5] fails as soon as the vehicle moves faster than $7\,\mathrm{m/s}$ and the RMSE thus increases to $10.14\,\mathrm{m/s}$ and $235\,^\circ/\mathrm{s}$.

In contrast to straight-line driving, Fig. 6 shows the result for cornering, with ground truth data shown in Fig. 6a and ego-motion estimation errors shown in Fig. 6b.

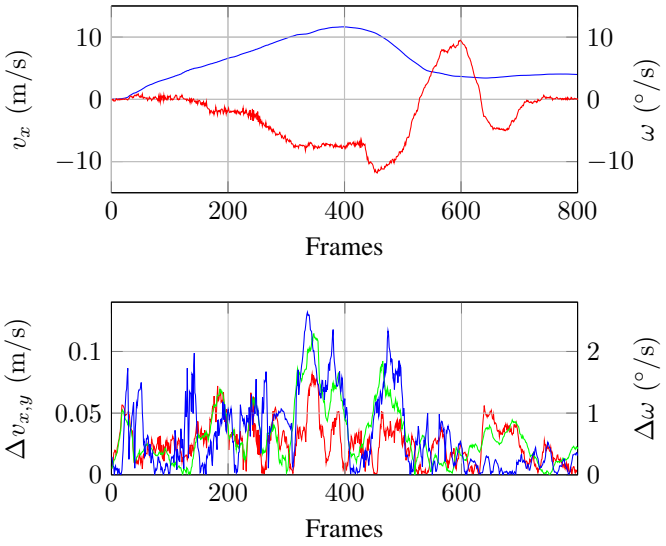


Fig. 6. Cornering at high speed. Ground truth velocity (top), estimation error (bottom) with $v_x$, $v_y$, and $\omega$.

Again, the vehicle speed is significantly higher than $v^{\mathrm{r}}_{\mathrm{max}}$. The RMSE for this measurement is smaller than $0.045\,\mathrm{m/s}$ and $0.5\,^\circ/\mathrm{s}$. Thus, it can be shown that a reliable velocity estimation in three DoF is possible for both straight and curved runs and that the velocity components can be separated unambiguously.

*Robustness*

The robustness depends significantly on the number of sensors and the ratio between maximum vehicle speed $v$ and the maximum measurable radial speed $v^{\mathrm{r}}_{\mathrm{max}}$. For the comparison, the straight-line drive from Fig. 5a in the frame interval $[400, 600]$ is considered, since the highest vehicle speeds occur during this interval. For the robustness analysis, only every $t$-th ramp is evaluated ($t \in \{1, 2, 4, 8, 16\}$), reducing $v^{\mathrm{r}}_{\mathrm{max}}$ by a factor of $t$. The result is shown in Fig. 7.

Once $N \geq 3$ sensors are used, the quality of velocity estimation is almost constant up to a lower limit of $v^{\mathrm{r}}_{\mathrm{max}} \approx 0.6\,\mathrm{m/s}$ ($k = 8$). As soon as only every 16-th ramp is used and thus $v^{\mathrm{r}}_{\mathrm{max}} \approx 0.3\,\mathrm{m/s}$ holds, no reliable velocity estimation can be performed anymore. Furthermore, it can be seen from Fig. 7 that the robustness decreases significantly as soon as only $N=2$ sensors are used, and a double $v^{\mathrm{r}}_{\mathrm{max}}$ must be available to obtain similar accuracies.

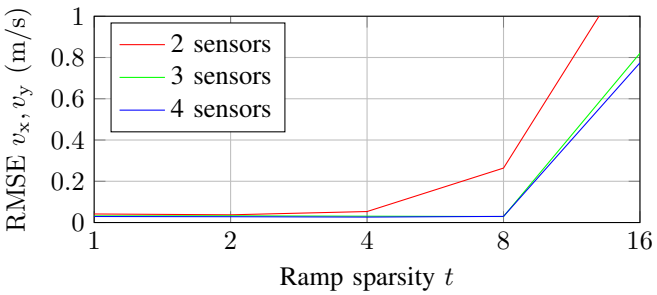


Fig. 7. Robustness comparison of different numbers of sensors and different maximum unambiguous measurable radial velocities.

## V. Conclusion

An algorithm for instantaneous ego-motion estimation without a priori knowledge or tracking and for velocities multiple times higher than the unambiguously detectable radial velocity of the radar system was presented. Its robustness regarding the number of sensors used in the network was analysed. It was shown that vehicle speeds that were more than 35 times higher than the maximum unambiguously measurable radial speed could be reliably estimated with a $\mathrm{RMSE}_{\mathrm{v}_{x,y}} < 0.05\,\mathrm{m/s}$, in all three DoFs.

## References


[1] Z. Qu, H. Gao, and Y. Zhu, "Research on High-accuracy Position Prediction Algorithm in Online Game," in *Int. Symp. on Electron. Commerce and Secur.*, 2008, pp. 78–81.

[2] S. Lupfer, M. Rapp, K. Dietmayer, P. Brosseit, J. Lombacher, M. Hahn, and J. Dickmann, "Increasing FastSLAM Accuracy for Radar Data by Integrating the Doppler Information," in *IEEE MTT-S Int. Conf. Microw. Intell. Mobil. ICMIM*, March 2017, pp. 103–106.

[3] S. H. Cen and P. Newman, "Precise Ego-Motion Estimation with Millimeter-Wave Radar Under Diverse and Challenging Conditions," in *IEEE Int. Conf. Robot. Autom. (ICRA)*, 2018, pp. 6045–6052.

[4] D. Kellner, M. Barjenbruch, J. Klappstein, J. Dickmann, and K. Dietmayer, "Instantaneous Ego-Motion Estimation Using Doppler Radar," in *16th IEEE Intell. Transp. Syst. Conf. (ITSC 2013)*, 2013, pp. 869–874.

[5] D. Kellner, M. Barjenbruch, J. Klappstein, J. Dickmann, and K. Dietmayer, "Instantaneous Ego-Motion Estimation Using Multiple Doppler Radars," in *IEEE Int. Conf. Robot. Autom. (ICRA)*, May 2014, pp. 1592–1597.

[6] M. Steiner, O. Hammouda, and C. Waldschmidt, "Ego-Motion Estimation using Distributed Single-Channel Radar Sensors," in *IEEE MTT-S Int. Conf. Microw. Intell. Mobil. (ICMIM)*, Apr. 2018, pp. 1–4.

[7] F. Roos, J. Bechter, N. Appenrodt, J. Dickmann, and C. Waldschmidt, "Enhancement of Doppler Unambiguity for Chirp-Sequence Modulated TDM-MIMO Radars," in *IEEE MTT-S Int. Conf. Microw. Intell. Mobil. (ICMIM)*, 2018, pp. 1–4.

[8] J. Bechter, F. Roos, and C. Waldschmidt, "Compensation of Motion-Induced Phase Errors in TDM MIMO Radars," *IEEE Microw. Wirel. Compon. Lett.*, vol. 27, no. 12, pp. 1164–1166, 2017.

[9] Y. Lin, T. Guo, M. Guo, and Y. Fu, "Motion Compensation for SAA FMCW Radar Based on Specific Switching Scheme," *Appl. Sci.*, vol. 9, no. 17, 2019.

[10] V. Winkler, "Range Doppler Detection for Automotive FMCW Radars," in *Eur. Microw. Conf.*, Oct. 2007, pp. 1445–1448.

[11] *Trimble Universale Totalstation*, 2018.